

Extracellular matrix proteins as temporary coating for thin-film neural implants

This content has been downloaded from IOPscience. Please scroll down to see the full text.

2017 J. Neural Eng. 14 014001

(<http://iopscience.iop.org/1741-2552/14/1/014001>)

View [the table of contents for this issue](#), or go to the [journal homepage](#) for more

Download details:

IP Address: 134.58.253.57

This content was downloaded on 09/01/2017 at 13:12

Please note that [terms and conditions apply](#).

Note

Extracellular matrix proteins as temporary coating for thin-film neural implants

Frederik Ceyskens^{1,5,6}, Marjolijn Deprez^{2,5}, Neill Turner³, Dries Kil¹,
Kris van Kuyck², Marleen Welkenhuysen⁴, Bart Nuttin²,
Stephen Badylak³ and Robert Puers¹

¹ Department of ESAT-MICAS, KULeuven, Leuven, Belgium

² Laboratory of Experimental Neurosurgery and Neuroanatomy, KULeuven, Leuven, Belgium

³ McGowan Institute for Regenerative Medicine, University of Pittsburgh, Pittsburgh, PA, USA

⁴ Imec, Leuven, Belgium

E-mail: fceyskens@esat.kuleuven.be

Received 14 July 2016, revised 30 October 2016

Accepted for publication 23 November 2016

Published 9 January 2017



Abstract

Objective. This study investigates the suitability of a thin sheet of extracellular matrix (ECM) proteins as a resorbable coating for temporarily reinforcing fragile or ultra-low stiffness thin-film neural implants to be placed on the brain, i.e. microelectrocorticographic (μ ECOG) implants. **Approach.** Thin-film polyimide-based electrode arrays were fabricated using lithographic methods. ECM was harvested from porcine tissue by a decellularization method and coated around the arrays. Mechanical tests and an *in vivo* experiment on rats were conducted, followed by a histological tissue study combined with a statistical equivalence test (confidence interval approach, 0.05 significance level) to compare the test group with an uncoated control group. **Main results.** After 3 months, no significant damage was found based on GFAP and NeuN staining of the relevant brain areas. **Significance.** The study shows that ECM sheets are a suitable temporary coating for thin μ ECOG neural implants.

Keywords: coatings, resorbable carrier, ECM, temporary reinforcement, ECOG, neural implants

(Some figures may appear in colour only in the online journal)

1. Introduction

Looking at the historic contributions of i.a. Galvani and Edgar Adrian [1], it is clear that the coupling of human-made electric devices to the nervous system is a centuries-old topic. Nevertheless, brain-machine interfacing and in particular the

pursuit of long-lasting, high-speed, high-resolution direct electrical communication with the brain is still a major challenge for scientists and engineers.

Plenty of work has pushed the state of the art forwards. Such work includes the introduction of monolithic needle probes or needle probe arrays penetrating the brain surface [2–6] and flexible electrode arrays for measuring microelectrocorticographic (μ ECOG) signals on the brain surface [7, 8]. More recently, versions of both needle probe arrays and μ ECOG arrays that include integrated electronics have been demonstrated as well, improving the channel count even further [9–12].

However, increasing the channel count is not the only issue to solve as scar tissue tends to build up around the implant.

⁵ Contributed equally to this work.

⁶ Author to whom any correspondence should be addressed.



Original content from this work may be used under the terms of the [Creative Commons Attribution 3.0 licence](https://creativecommons.org/licenses/by/3.0/). Any further distribution of this work must maintain attribution to the author(s) and the title of the work, journal citation and DOI.

This increases the distance between the viable neural tissue and the implant, increases the contact impedance and limits the ultimate resolution [13]. An important insight in the strive towards well-performing high-resolution chronic neural implants has been the discovery of the detrimental effects of motion of the implant with respect to the brain, which is much softer than any artificial electrode structure [14, 15]. Therefore, researchers have introduced ‘floating’ needle implants that are attached to the outside by a flexible connector [16, 17], or have emphasized the importance of mechanically flexible implants. If an implant is made so flexible that insertion becomes problematic, this can be resolved by temporary reinforcement by a biocompatible water-soluble or resorbable material, or with another type of temporary reinforcement [18–21]. An alternative is injection while dispersed in a liquid [22].

A second important aspect that causes the buildup of scar tissue is the response of the immune system to the implant’s surface, which is perceived as a foreign body. Several approaches to limit this effect have been published, including the release of cortisones [23] and the coating of the implant with molecules such as laminin [24, 25] or neuron-specific adhesion factors such as L1 [26].

In this work, we will study the use of extracellular matrix (ECM) proteins in neural implants positioned on the brain. We will show the potential of thin ECM sheets as temporary reinforcement material that allows inserting implants too fine to support themselves during insertion. The ECM naturally occurs as a scaffold structural support for the body’s cells in all tissue types and also plays an important function in cell signaling, acting e.g. as a reservoir for growth factors [27]. ECM sheets can be harvested from animal tissue by a variety of decellularization processes [28], and can then be used in a range of tissue engineering applications. ECM proteins are highly conserved across mammalian species and when properly decellularized these biologic scaffolds are well accepted by the body, even if the source tissue is xenogenic. For example, biologic scaffolds derived from porcine small intestine submucosa (SIS) are commercially available for use in human surgery [29]. ECM coatings have also been shown to reduce the chronic inflammatory response to implanted polypropylene meshes [30]. Moreover, a hydrogel based on porcine bladder ECM has also been applied successfully in animal tests to reduce damage after traumatic brain injury [31]. Recently, neural tissue-based ECM has also come under investigation for that target application though the *in vivo* performance does not yet clearly exceed that of non-neural ECM [32, 33]. SIS ECM has been used successfully as dura mater repair material [34]. Based on the latter results, we have selected SIS for use in our neural implant coating experiment as environment it is applied in is the same.

2. Methods

2.1. Neural implant design

The implants used as in the test and control group of this study were designed to be used for electric measurements and stimulation in cavities in the brain in a related research project [35].

These electrode array implants are composed of ‘islands’ that carry one electrode each and are connected with spring-like structures that also contain the conductors to allow bendability and in-plane stretchability. The implants consist of two layers of polyimide (PI) insulation, between which platinum conductors and electrodes are sandwiched. The electrode arrays were designed using finite element (FE) simulation to have similar flexibility and stretchability as those of a previous generation with lower area [21]. The area of the designed electrode array excluding the connector is $5 \times 5 \text{ mm}^2$.

The implants are $7 \mu\text{m}$ thick in total and therefore very flexible, but still strong enough to be used without reinforcing coating. Therefore, implants not coated with ECM can serve as a reference in the *in vivo* experiments. This does not defeat the purpose of the experiment which is to show that the ECM material can be used as biocompatible temporary reinforcement: an even thinner PI structure will show similar or better biocompatibility behavior when ECM-coated because the surface properties will be the same and possible mechanical irritation will only be lower.

The layout of the electrode arrays is shown in figure 1. This figure also shows a 4×4 electrode array resulting from the fabrication process, after it has been lifted off from the wafer it was fabricated on and an Omnetics connector was mounted.

The lithographic process used to fabricate the electrode arrays is detailed in another publication [36]. Basically, a silicon substrate is coated with an aluminum sacrificial layer on which the first PI layer (Dupont PI2611) is deposited by spin coating and partially cured by heating it to $200 \text{ }^\circ\text{C}$. This was shown to lead to an improved insulation performance compared to a full curing of the layer at this step [36]. Then, the platinum conductors are deposited by sputtering and patterned by a liftoff process. Thereafter, the second PI layer is deposited and the assembly is fully cured by heating to $350 \text{ }^\circ\text{C}$. In a further step, the PI layers are patterned and the electrode contacts are opened using reactive ion etching. Then, the devices are removed from the carrier wafer. In a final step, the Omnetics connector is mounted by soldering and the connector pins and bond pads are electrically insulated using H54 epoxy cured at $150 \text{ }^\circ\text{C}$ for 1 h.

2.2. Neural implant coating

SIS ECM sheets were isolated from freshly harvested porcine gut tissue by mechanically scraping off the surrounding tissues, followed by rinsing in 0.1% peracetic acid and PBS as previously described [37] in more detail. After production, the SIS was freeze dried and stored until needed for implant coating. Before coating, the implant was disinfected with 70% isopropyl alcohol. A single SIS sheet was then cut to a size 2 mm larger than the outline of the implant, rehydrated with saline and wrapped around the implant such that it would cover both sides. The abluminal side of the SIS was placed facing inside. The laminate was then put on a block of porous glass, covered with a Teflon foil and put in a vacuum chamber for drying while a pressure of about 1 bar was applied by putting an appropriate steel block on top, coated with anti-stick Teflon spray. The drying time was 3 h. After drying, the SIS

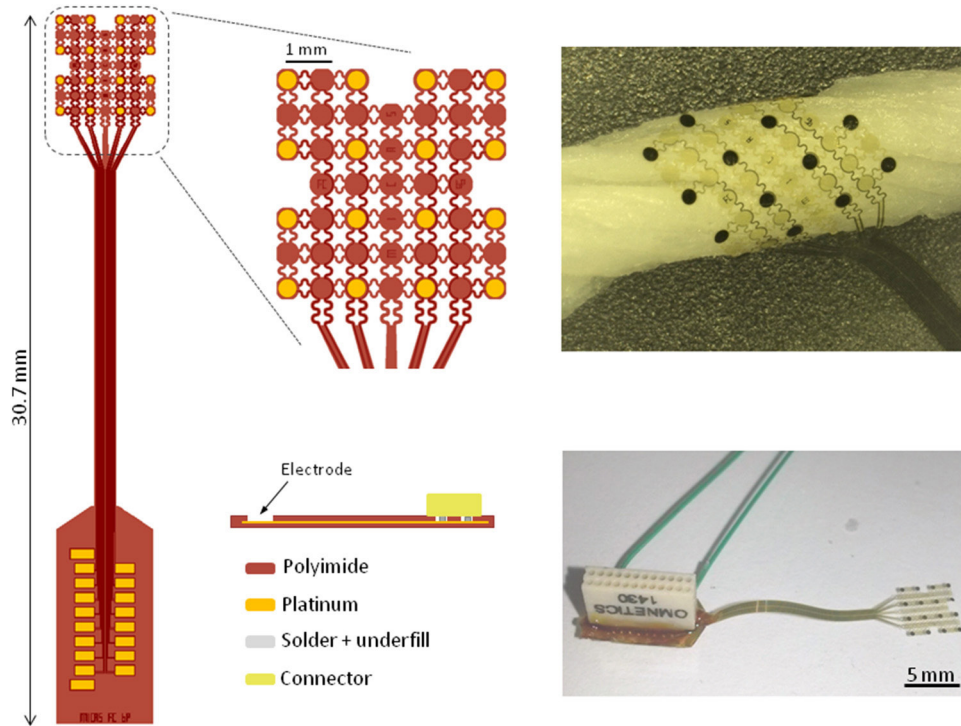


Figure 1. Left: layout of the 4 × 4 electrode array used. Lower middle: cross section. Top right: fabricated electrode array, wrapped around a 2 mm diameter mock nerve. Configuration of electrode and wires is well visible. Lower right: assembled electrode array.

coating was cut to a size about 0.5 mm larger than the outline of the electrode array using surgical scissors. A coated implant is shown in figure 2. Before implantation, the coated implants were sterilized using ethylene oxide vapor for 20h at 38 °C.

2.3. Micromechanical testing

In order to assess the level of mechanical reinforcement obtainable by ECM coating as described, four additional electrode arrays were fabricated and coated using the procedure outlined in sections 2.1 and 2.2. The dimensions of the coating layer were measured using a caliper and mechanical thickness gauge.

Four uncoated implants were taken as a reference. The connector and hind part of the samples were glued to an aluminum oxide substrate, leaving the electrode array part sticking out over the edge of the substrate. A Femtotools FTA-M02 micro-mechanical testing device (figure 3) was then used to displace the freestanding part of the samples in the out-of-plane direction and measure the reaction force during displacement. Out-of-plane loading mimics the forces on the implant during and after insertion well, as is clear from figure 4. The underlying bending stiffness k (equaling applied force/displacement) was determined from these measurements by linear interpolation. The Young’s modulus E of the materials was then determined based on the well-known formula for bending of a beam under a point load:

$$E = \frac{k \cdot L^3}{3 \cdot I} \tag{1}$$

With I the area moment of inertia:

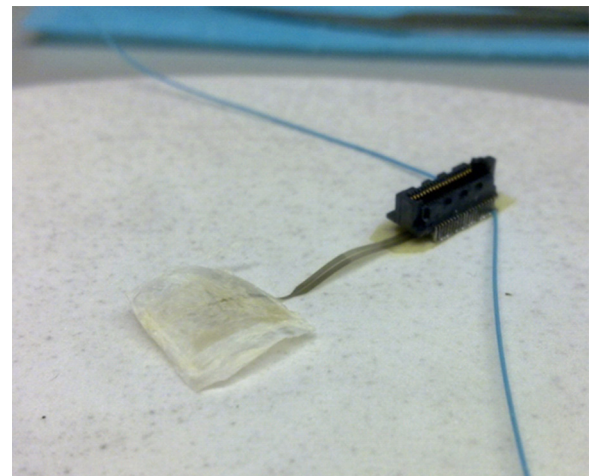


Figure 2. Coated implant.

$$I = \frac{b \cdot h^3}{12} \tag{2}$$

In these equations, L is the distance between the support and the contact point of the indenter tip, b is the measured width of the sample and h is the sample thickness. The ECM thickness was to be measured for every sample as there is a cubic dependence and the thickness can be expected to vary as the ECM is from a natural source. As the stiffness of the coating is orders of magnitude higher than the stiffness of the uncoated implant, the presence of the latter in the center of the coating can be ignored when determining the mechanical properties of the coated implants. The basic shape of the uncoated implants is more complicated than a simple beam.



Figure 3. Measuring bending stiffness using the Femtools FTA-M02 micromechanical testing device. Inset: close-up of indenter tip with force sensor, pushing down on the electrode array.

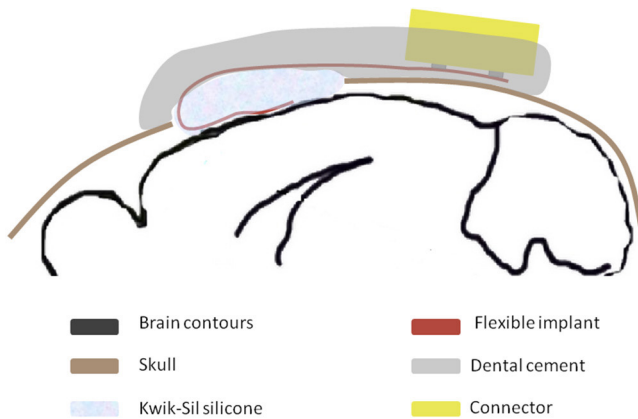


Figure 4. Graph showing how the implant is positioned on the brain.

Therefore, finite element simulation (Comsol Multiphysics, Mindlin plate 2D model) was used to determine the Young's modulus there with more precision, supplementing the simple beam approximation.

2.4. *In vivo* experiments

In vivo experiments were performed on male Wistar rats ($n = 18$) weighing approximately 250 g upon arrival. They were housed in pairs, separated from each other by a cage divider, in an animal room with a 14:10 light:dark cycle (lights on at 07h00) and a constant temperature of 20 °C. Animals received ad libitum food and water. The research project was in accordance with the Belgian and European laws, guidelines and policies for animal experimentation, housing and care (Belgian Royal Decree of 29 May and European Directive 2010/63/EU on the protection of animals used for scientific purposes of 20 October 2010). Rats were divided into a test group ($n = 9$), which received an ECM-coated implant as described above and a control group ($n = 9$) that received a non-coated implant.

They were anesthetized with a mixture of ketamine (Nimatek, Eurovet Animal Health B.V., Bladel, The Netherlands; 60 mg kg⁻¹; i.p.) and medetomidine hydrochlorate (NarcoStart, Kela Veterinaria NV, Sint-Niklaas, Belgium; 0.2 mg kg⁻¹; i.p.) and were then secured in a stereotactic frame. A burr hole was made

Table 1. Results of mechanical measurements.

	Mean	Standard error
Coating thickness (μm)	211	18
Bending stiffness, uncoated (N m^{-1})	0.019	0.004
Bending stiffness, coated (N m^{-1})	10.6	4.1
Young's Modulus of PI (GPa)	7.7	1.8
Young's modulus of ECM (GPa)	0.15	0.04

over the primary motor cortex of the right brain hemisphere at the following coordinates: $A = 3$ mm; $P = 2$ mm; $L = 0.5$ – 4.5 mm. The electrode was then implanted on the dura mater, which is very thin in rats, overlying the healthy motor cortex. The coated electrodes were moistened with saline before implantation. After implantation, the electrode array was covered with a layer of Kwik-Sil silicone (World Precision Instruments, USA) after which the bore hole and connector were enclosed using UV curing dental cement (Nanofil Flowable AT&M Biomaterials Co., Beijing, China), after which the skin was sutured. The rats received pain medication and remained on a heating plate (36 °C) until regaining consciousness. A schematic of the electrode placement is shown in figure 4.

Three animals of each group were perfused at the following time points: one week post implantation, 3 weeks post implantation, 13 weeks post implantation. Animals were perfused intracardially, first with 10% sucrose in distilled water and then with 4% formaldehyde in distilled water. The brains were dissected and submerged in 4% formaldehyde in distilled water during 24 h after which they were transferred to a 20% sucrose solution with sodium azide. The samples were kept at 4 °C until cryosection. After fast freezing at -50 °C on the cryostat chuck, twenty micron thick cryosections were made at a temperature of -20 °C.

2.5. *GFAP* and *NeuN* staining

GFAP and NeuN staining was then used to test for a potential increase in glial cell density (immune response) and to compare viable neuron densities, respectively. For this purpose, we used the following protocol: after rehydration in PBS, the sections were incubated in 20% goat serum and 0.2% Triton X-100 for 2 h. Then, a mixture of 1:100 mouse NeuN antibody dilution and a 1:500 rabbit GFAP antibody dilution was added and incubated overnight. Then, the mixture was removed and the slides were washed 3 times in PBS for 15 min. Then the secondary antibodies, Alexa Fluor 568 goat anti-mouse and Alexa Fluor 633 goat anti-rabbit (both in 1:500 dilution) were added and incubated for 2 h. The secondary antibodies were then washed away in PBS in two steps of 10 min. Before finally attaching a coverslip, the sections were coated with a drop of Vectashield DAPI.

2.6. *Data analysis*

After staining, samples were inspected using a confocal laser scanning microscope. A 4.2 mm \times 2.5 mm frame centralized under the location of the implant was imaged with 8-bit

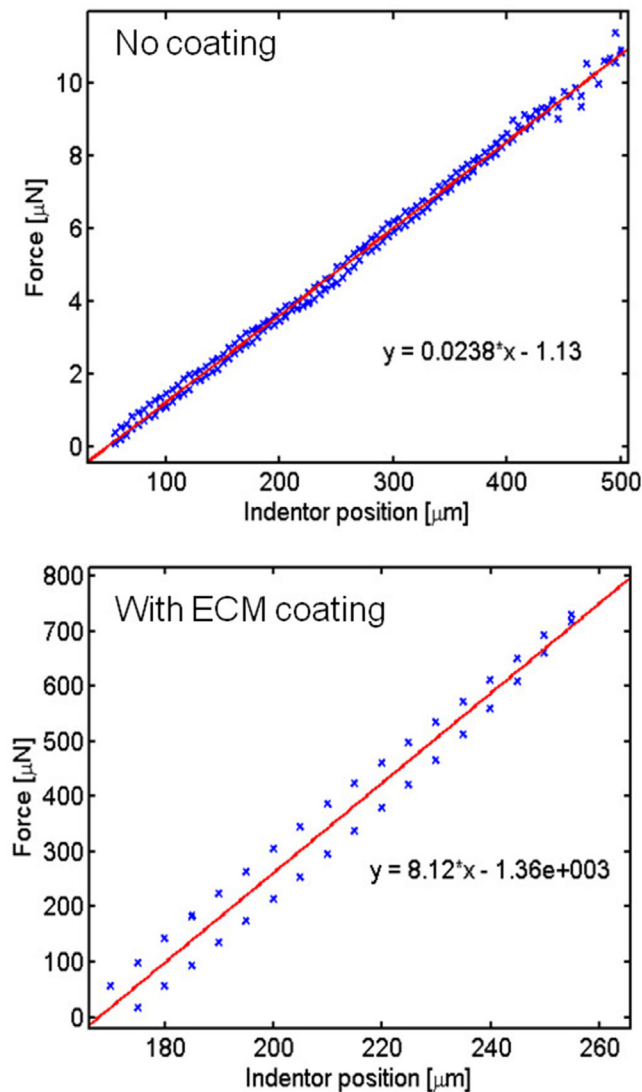


Figure 5. Measured applied displacement versus measured force for a non-coated (top graph) and a coated (bottom graph) implant. The red line shows the linear fit of the data.

grayscale color depth, as well as the corresponding untouched contralateral area of the brain on the same section to be used as the reference. In the analyses, the ratio between the averaged intensity of the left and right image was used, which reduces the effect of slide-to-slide variation. Furthermore, before averaging, a set threshold was applied to reduce background noise. In the case of the GFAP stain, the threshold was determined ad hoc based on the intensity histogram of the parts of the image outside the tissue by selecting a value that removed most of this background noise, i.e. three standard deviations from the peak center of the average histogram. In the case of the NeuN stain, the threshold was increased until the neural cell bodies, which are normally clearly visible, start to disappear.

In order to statistically test for equivalence, the common confidence interval approach [38] was used at the 0.05 significance level. The test requires the definition of an equivalence interval. If the confidence interval (CI) of the difference between the averages of the test and control group fully lies within the equivalence interval, the two groups are considered

equivalent. The equivalence interval was set at $\pm 10\%$. To estimate the number of degrees of freedom of the combination of the two groups, which is necessary for the equivalence test, the Welch-Satterthwaite equation was used.

3. Results

3.1. Mechanical measurements

Measurements were performed such as described in section 2.3 and summarized in table 1. The measurements showed that the uncoated implants had an average thickness of $7 \mu\text{m}$, versus $211 \mu\text{m}$ for the coated implants. The average width of the coating layer was 5.7 mm . Micromechanical testing revealed an average bending stiffness of 0.019 N m^{-1} for the uncoated implants. Coating increased this average bending stiffness 558 fold to 10.6 N m^{-1} (figure 5). By fitting the measurements on a finite element model as described in section 2.3 the Young's modulus of the polyimide was determined to be 7.7 GPa . This lies within the range of values reported in the literature, $5.8\text{--}8.5 \text{ GPa}$ [39, 40]. The Young's modulus of the ECM layer was measured to be only 0.15 GPa . Thus, the reinforcement effect of the coating is mainly due to its thickness.

3.2. Histology

During dissection of the brain, we observed that the burr hole was closed entirely with new bone tissue. The implanted electrode array was always found attached to the inside surface of the regrown bone and was not connected firmly to the brain. Therefore, the histological slices made for analysis do not contain the electrode itself. Still, as observed in our previous work, an implant positioned in this way can cause significant neural damage if e.g. an inflammation reaction is present [21].

Visual inspection of the histological slides revealed no appreciable brain damage, which normally manifests itself as a cavity under the implant location. Examples are shown in figure 6. It should be noted that in our previous work, in which we used a chitosan coating instead of an ECM coating, such a cavity was present [21]. An exception was seen in two rats that were euthanized one week after electrode implantation. Only in these rats we noticed significant bleeding in the brain during surgery which is therefore the most likely cause of the damage. As the test group became too small when leaving out the two rats, we did not analyze the 7 samples further.

After imaging the slides by laser confocal microscopy, image processing and data analysis was done as described in section 2. The intensity threshold value was set using the procedure outlined before, which resulted in a value of 60 for the NeuN stain and 25 for the GFAP stain. The intensity measurements are summarized in figure 7 (3 weeks after implantation) and figure 8 (3 months after implantation). In these figures, the left column shows the measured intensities per group and per hemisphere while the right column shows the ratio between the intensity in the right hemisphere—where the implant was located—and the untouched left hemisphere of the rats. The ratios are clearly showing much less variation than the absolute data. The 95% confidence interval of the GFAP ratios lies above 1 both for the

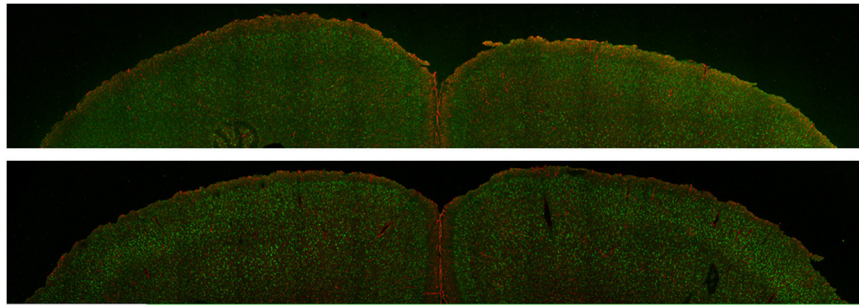


Figure 6. Example pictures of resulting immunohistological staining. No obvious brain damage in the form of cavities is visible after 3 months. NeuN stain is green, GFAP is red. Top: rat from the test group. Bottom: from control group.

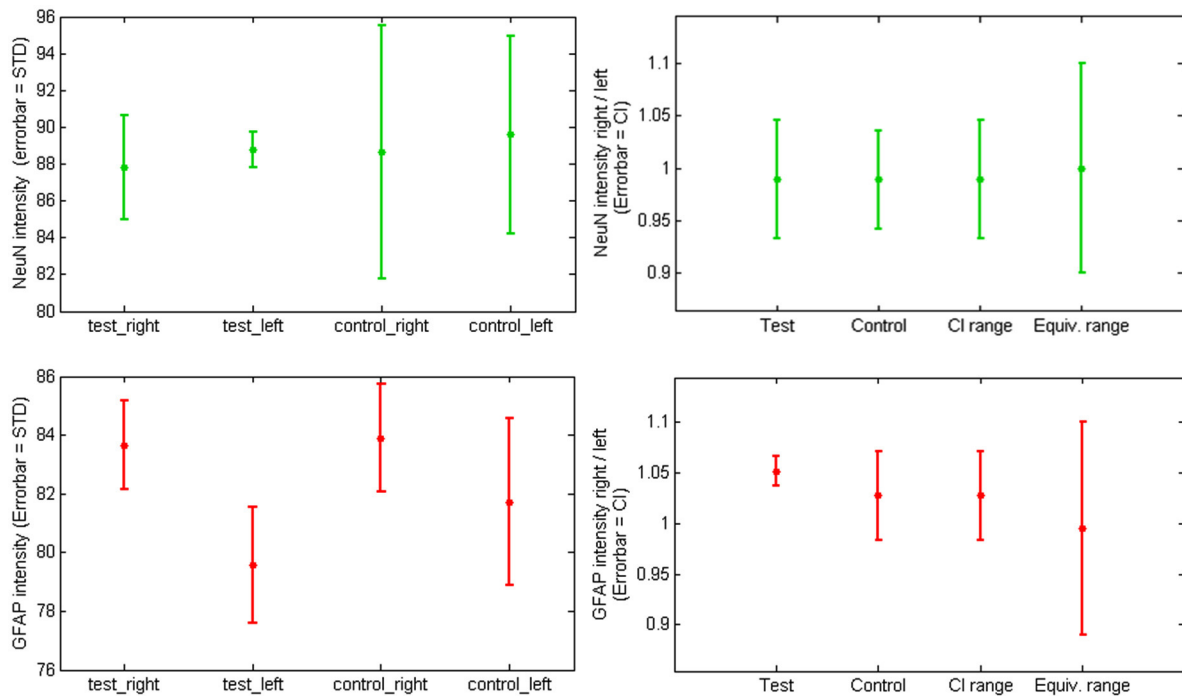


Figure 7. Analysis results for samples taken after 3 weeks, showing NeuN (top row) and GFAP (bottom row) measured intensities. The left graphs display the measurements for the two hemispheres separately (average and standard deviation shown), while the right graphs show the average ratio between the measured intensity right and left per group, together with the 95% confidence interval. CI range, the combined range of the test and control CIs, lies within the predefined equivalence range. Therefore, test and control groups can be considered equivalent.

test and control group, indicating an increased glial cell response in both groups. However, the equivalence test shows that there is no significant difference in glial cell response between the non-ECM coated control group and the test group within the specified range of $\pm 10\%$. The difference between the means is just a few percent. Furthermore, the graphs show no indication of a decreased neuron density based on the NeuN stain after 3 weeks as well as after 3 months. Finally, the neuron density in the test and the control groups is shown to be statistically equivalent.

4. Discussion

A group of ECM-coated thin film neural implants was compared with a non-coated control, in a situation where the implants were put directly on the dura of the brain. Based on confidence intervals at the 0.05 significance level with an equivalence range of $\pm 10\%$, we conclude that the viability

of nearby neurons and glial cell response were not different between the test and control group. Visual inspection of brain slices also did not show any cavities or other signs of damage. Therefore, the presented technique is a good candidate for temporarily supporting neural implants that are by themselves too flexible to be inserted into the body without support.

The investigated period of three months is sufficient, as most of the ECM will be absorbed by the body in two months [41]. Compared with most temporary reinforcement materials found in the literature cited in the introduction (silk, carboxymethyl cellulose, chitosan) the constituents of the ECM will be the very same the intracellular environment naturally contains and will elicit a benign response. Another advantage is that ECM sheets are already commercially available, approved for human use.

There are several aspects that are left for further investigation. As with all coatings, the presence of the temporary ECM layer can influence the electrode performance shortly

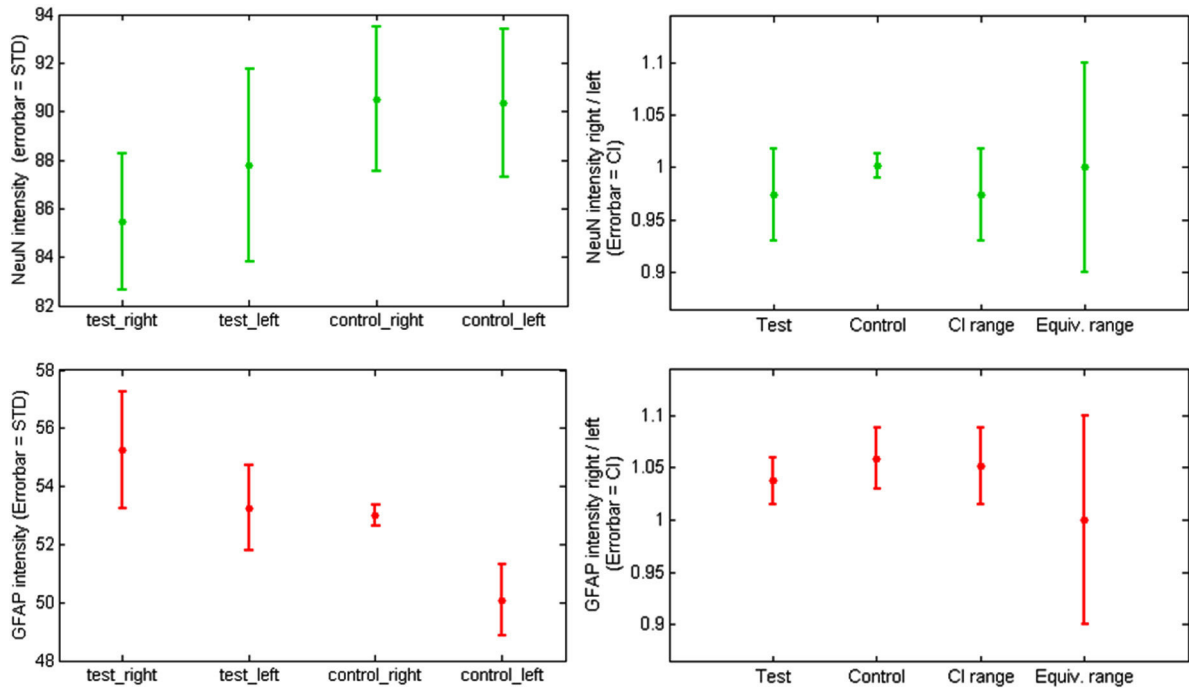


Figure 8. Analysis results for samples taken after 3 months. The interpretation is similar to that in figure 7.

after implantation. Therefore, the electrical performance of the implants should be compared with that of uncoated implants in a longitudinal study. A second point for further study is the application of temporary reinforcement with ECM in a more challenging environment such as directly in the brain parenchyma, in a healthy or diseased region. For example, in other recent work, it was shown that bladder-derived ECM gel injected in the brain is well tolerated and can even reduce lesion size after trauma [31]. Therefore, it is possible that ECM coating reduces trauma caused by insertion in the brain. This could also be the case in existing brain trauma, such as lesion cavities formed after hemorrhage.

The coating material used does not need to be limited to the already commercially available and well-studied material used here. Several research groups work on improving the state of the art of regenerative medicine for the brain and study new scaffold materials specific for neural applications. The group of new materials under study comprises both natural, decellularized neural tissue [42] as well as newly synthesized hydrogel materials [43, 44].

As the methods shown in this paper can be adapted to other coating materials, results of the current research in regenerative medicine for the brain can possibly be put to use to improve neural interfacing devices as well. Moreover, regenerative medicine research could also benefit from integrating electrodes in implanted scaffolds as they allow real-time study of electrical signals.

5. Conclusion

In short, the current work indicates that ECM sheets are a suitable temporary coating material for reinforcing thin neural implants that are to be placed on the brain. Coating of neural

implants with materials investigated in regenerative medicine research is not only a promising way to improve neural interfacing devices, but also opens up new prospects for multimodal regenerative medicine research in which electrical measurements or stimulation are combined with bioactive scaffolds for inducing and studying tissue regeneration.

Acknowledgments

This research was made possible by Frederik Ceysens' research fellowship from FWO-Flanders and the KULeuven IDO/12/024 grant, and was further supported by the Hercules Foundation for heavy equipment (AKUL 034 and ZW1115). The research leading to these results has received funding from the European Research Council under the European Union's Seventh Framework Programme (FP7/2007-2013)/ERC grant agreement n° 340931.

References

- [1] Adrian E D 1928 *The Basis of Sensation* (New York: W W Norton & Co) p 122
- [2] Prohaska O, Olcaytug F, Womastek K, Petsche H 1977 A multielectrode for intracortical recordings produced by thin-film technology *Electroencephalogr. Clin. Neurophysiol.* **42** 421–2
- [3] Peeters E, Puers B, Sansen W, Gybels J and De Sutter P 1991 A two-wire, digital output multichannel microprobe for recording single-unit neural activity *Sensors Actuators* **4** 217–23
- [4] Aarts A, Srivannavit O, Wise K D, Yoon E, Puers R, Hoof C V and Neves H P 2011 Fabrication technique of a compressible biocompatible interconnect using a thin film transfer process *J. Micromech. Microeng.* **21** 074012

- [5] Bai Q, Wise K and Anderson D 2000 A high-yield microassembly structure for three-dimensional microelectrode arrays *IEEE Trans. Biomed. Eng.* **47** 281–9
- [6] Blanche T, Spacek M, Hetke J and Swindale N 2005 Polytrodes: high-density silicon electrode arrays for large-scale multiunit recording *J. Neurophysiol.* **93** 2987
- [7] Shamma-Donoghue S A, May G A, Cotter N E, White R L and Simmons F B 1982 Thin-film multielectrode arrays for a cochlear prosthesis *IEEE Trans. Electron Devices* **29** 136–44
- [8] Rubehn B, Bosman C, Oostenveld R, Fries P and Stieglitz T 2009 A MEMS-based flexible multichannel ECoG-electrode array *J. Neural Eng.* **6** 036003
- [9] Wise K, Anderson D, Hetke J, Kipke D and Naja K 2004 Wireless implantable microsystems: high-density electronic interfaces to the nervous system *Proc. IEEE* **92** 7697
- [10] Viventi J *et al* 2011 Flexible, foldable, actively multiplexed, high-density electrode array for mapping brain activity *in vivo Nat. Neurosci.* **14** 1599–605
- [11] Torfs T *et al* 2011 Two-dimensional multi-channel neural probes with electronic depth control *IEEE Trans. Biomed. Circuits Syst.* **5** 403–12
- [12] Pothof F, Galchev T, Patel M, Herbawi A S, Paul O and Ruther P 2015 128-channel deep brain recording probe with heterogeneously integrated analog CMOS readout for focal epilepsy localization *Solid-State Sensors, Actuators and Microsystems (Transducers) (Anchorage, AK, 21–25 June 2015)*
- [13] Xindong L, McCreery D B, Carter R R, Bullara L, Yuen T G H and Agnew W F 1999 Stability of the interface between neural tissue and chronically implanted intracortical microelectrodes *IEEE Trans. Rehabil. Eng.* **7** 315–26
- [14] Rousche P J, Pellinen D S, Pivin D P, Williams J C, Vetter R I and Kipke D R 2001 Flexible polyimide-based intracortical electrode arrays with bioactive capability *IEEE Trans. Biomed. Eng.* **48** 361–71
- [15] Kim Y T, Hitchcock R W, Bridge M J and Tresco P A 2004 Chronic response of adult rat brain tissue to implants anchored to the skull *Biomaterials* **25** 2229–37
- [16] Vetter R J, Williams J C, Hetke J F, Nunamaker E and Kipke D R 2004 Chronic neural recording using silicon-substrate microelectrode arrays implanted in cerebral cortex *IEEE Trans. Biomed. Eng.* **51** 896–904
- [17] Lee K K *et al* 2004 Polyimide-based intracortical neural implant with improved structural stiffness *J. Micromech. Microeng.* **14** 32–7
- [18] Kozai T D Y and Kipke D R 2009 Insertion shuttle with carboxyl terminated self-assembled monolayer coatings for implanting flexible polymer neural probes in the brain *J. Neurosci. Methods* **184** 199–205
- [19] Kim D *et al* 2010 Dissolvable films of silk fibroin for ultrathin conformal bio-integrated electronics *Nat. Mater.* **9** 511–7
- [20] Kozai T D Y, Gugel Z, Li X, Gilgann P J, Khilwani R, Ozdoganlar O B, Fedder G K, Weber D J and Cui T 2014 Chronic tissue response to carboxymethyl cellulose based dissolvable insertion needle for ultra-small neural probes *Biomaterials* **35** 9255–68
- [21] Ceyskens F, van Kuyck K, Vande Velde G, Welkenhuysen M, Stappers L, Nuttin B and Puers R 2013 Resorbable scaffold based chronic neural electrode arrays *Biomed. Microdevices* **15** 481–93
- [22] Huosong H, Fu T M, Zhou T, Schuhmann T G, Huang J and Lieber C M 2015 Syringe injectable electronics: precise targeted delivery with quantitative input/output connectivity *Nano Lett.* **15** 6979–84
- [23] Reecha W, Lagenaur C F and Cui T 2006 Electrochemically controlled release of dexamethasone from conducting polymer polypyrrole coated electrode *J. Control. Release* **110** 531–41
- [24] Wei H, McConnell G C and Bellamkonda R V 2006 Nanoscale laminin coating modulates cortical scarring response around implanted silicon microelectrode arrays *J. Neural Eng.* **3** 316
- [25] Massia S P, Holecko M M and Ehteshami G R 2004 *In vitro* assessment of bioactive coatings for neural implant applications *J. Biomed. Mater. Res. A* **68** 177–86
- [26] Erdrin A, Lagenaur C F and Cui X T 2011 The surface immobilization of the neural adhesion molecule L1 on neural probes and its effect on neuronal density and gliosis at the probe/tissue interface *Biomaterials* **32** 681–92
- [27] Jones J I, Gockerman A, Busby W H, Camacho-Hubner C and Clemmons D R 1993 Extracellular matrix contains insulin-like growth factor binding protein-5: potentiation of the effects of IGF-I *J. Cell Biol.* **121** 679–87
- [28] Crapo P M, Gilbert T W and Badylak S F 2011 An overview of tissue and whole organ decellularization processes *Biomaterials* **32** 3233–43
- [29] Birgit A, Bär A, Haverich A and Hilfiker A 2013 Small intestinal submucosa segments as matrix for tissue engineering: review *Tissue Eng. B* **19** 279–91
- [30] Faulk D M, Londono R, Wolf M T, Ranallo C A, Carruthers C A, Wildemann J D, Dearth C L and Badylak S F 2014 ECM hydrogel coating mitigates the chronic inflammatory response to polypropylene mesh *Biomaterials* **35** 8585–95
- [31] Zhang L, Zhang F, Weng Z, Brown B N, Yan H, Ma X M, Vosler P S, Badylak S F, Dixon C E and Cui X T 2013 Effect of an inductive hydrogel composed of urinary bladder matrix upon functional recovery following traumatic brain injury *Tissue Eng. A* **19** 1909–18
- [32] Tukmachev D *et al* 2016 Injectable extracellular matrix hydrogels as scaffolds for spinal cord injury repair *Tissue Eng. A* **22** 306–17
- [33] DeQuach J A, Yuan S H, Goldstein L S and Christman K L 2011 Decellularized porcine brain matrix for cell culture and tissue engineering scaffolds *Tissue Eng. A* **17** 2583–92
- [34] Cobb M A, Badylak S F, Janas W, Simmons-Byrd A and Boop F A 1999 Porcine small intestinal submucosa as a dural substitute *Surg. Neurol.* **51** 99–104
- [35] Nica I G, Deprez M, Ceyskens F, van Kuyck K, Puers B, Nuttin B and Aerts J M 2015 Neuronal patterns in the cavity wall of lesions during gait cycle in a rat model of brain lesion cavities *Biosignals (Lisbon)* pp 289–94
- [36] Ceyskens F and Puers R 2015 Insulation lifetime improvement of polyimide thin film neural implants *J. Neural Eng.* **12** 054001
- [37] Badylak S F, Lantz G C, Coffey A and Geddes L A 1989 Small intestinal submucosa as a large diameter vascular graft in the dog *J. Surg. Res.* **47** 74–80
- [38] Esteban W and Nowacki A S 2011 Understanding equivalence and noninferiority testing *J. Gen. Intern. Med.* **26** 192–6
- [39] Sun Y, Lacour S P, Brooks R A, Rushton N, Fawcett J and Cameron R E 2009 Assessment of the biocompatibility of photosensitive polyimide for implantable medical device use *J. Biomed. Mater. Res. A* **90** 648–55
- [40] Rubehn B and Stieglitz T 2010 *In vitro* evaluation of the long-term stability of polyimide as a material for neural implants *Biomaterials* **31** 3449–58
- [41] Gilbert T W, Stewart-Akers A M and Badylak S F 2007 A quantitative method for evaluating the degradation of biologic scaffold materials *Biomaterials* **28** 147–50
- [42] Ghuman H, Massensini A R, Donnelly J, Kim S M, Medberry C J, Badylak S F and Modo M 2016 ECM hydrogel for the treatment of stroke: characterization of the host cell infiltrate *Biomaterials* **91** 166–81
- [43] Carballo-Molina O A and Velasco I 2015 Hydrogels as scaffolds and delivery systems to enhance axonal regeneration after injuries *Front. Cell. Neurosci.* **9** 13
- [44] Suri S and Schmidt C E 2010 Cell-laden hydrogel constructs of hyaluronic acid, collagen, and laminin for neural tissue engineering *Tissue Eng. A* **16** 1703–16